Published online 11 July 2018 *Nucleic Acids Research, 2018, Vol. 46, No. 15 7757–7771*
doi: 10.1093/nar/gky597

Trypanosoma brucei UMSBP2 is a single-stranded telomeric DNA binding protein essential for chromosome end protection

Olga Klebanov-Akopyan[1,†], Amartya Mishra[1,†], Galina Glousker[2], Yehuda Tzfati[2,*] and Joseph Shlomai[1,*]

[1]Department of Microbiology and Molecular Genetics, Institute for Medical Research Israel-Canada and Kuvin Center for the Study of Infectious and Tropical Diseases, The Hebrew University-Hadassah Medical School, Jerusalem 91120, Israel and [2]Department of Genetics, The Silberman Institute of Life Sciences, Edmond Safra Campus, The Hebrew University of Jerusalem, Jerusalem 91904, Israel

Received February 12, 2018; Revised June 02, 2018; Editorial Decision June 17, 2018; Accepted July 06, 2018

ABSTRACT

Universal minicircle sequence binding proteins (UMSBPs) are CCHC-type zinc-finger proteins that bind a single-stranded G-rich sequence, UMS, conserved at the replication origins of the mitochondrial (kinetoplast) DNA of trypanosomatids. Here, we report that *Trypanosoma brucei* TbUMSBP2, which has been previously proposed to function in the replication and segregation of the mitochondrial DNA, colocalizes with telomeres at the nucleus and is essential for their structure, protection and function. Knockdown of *TbUMSBP2* resulted in telomere clustering in one or few foci, phosphorylation of histone H2A at the vicinity of the telomeres, impaired nuclear division, endoreduplication and cell growth arrest. Furthermore, TbUMSBP2 depletion caused rapid reduction in the G-rich telomeric overhang, and an increase in C-rich single-stranded telomeric DNA and in extrachromosomal telomeric circles. These results indicate that TbUMSBP2 is essential for the integrity and function of telomeres. The sequence similarity between the mitochondrial UMS and the telomeric overhang and the finding that UMSBPs bind both sequences suggest a common origin and/or function of these interactions in the replication and maintenance of the genomes in the two organelles. This feature could have converged or preserved during the evolution of the nuclear and mitochondrial genomes from their ancestral (likely circular) genome in early diverged protists.

INTRODUCTION

Telomeres are protein–DNA structures that protect the ends of eukaryotic chromosomes from degradation and activation of the DNA damage response (DDR), and from repair activities such as homologous recombination (HR) and non-homologous end joining (NHEJ) (reviewed in (1)). Telomeric DNA consists of sequence-specific tandem DNA repeats and it ends with an essential G-rich single-stranded 3′-overhang. Critically short or otherwise dysfunctional telomeres activate DDR and cause cell cycle arrest or apoptosis. Specialized proteins bind the single- and double-stranded parts of the telomere and facilitate its replication and function. The 3′-overhang was suggested to form a special displacement loop termed telomere (t)-loop, via invasion of the telomeric double-stranded DNA (dsDNA) by the 3′ overhang, where it is protected and inaccessible to DDR factors (2). The 3′ overhang can be elongated by the enzyme telomerase to make up for losses caused by incomplete DNA replication and degradation. Specialized single-stranded telomeric binding proteins were found in various organisms to regulate the maintenance of the 3′-overhang, the activity of telomerase, the localization of the telomeres to the nuclear periphery, and the suppression of DDR (3–6). These proteins contain oligonucleotide/oligosaccharide-binding (OB) folds that are involved in single-stranded DNA (ssDNA) binding (7). Recently, a new telomere binding protein TZAP, which is involved in telomere length control, has been described (8). Binding of telomeres by this protein is mediated through its zinc finger domains.

Fundamental telomeric features are common between vertebrates and trypanosomatids (reviewed in (9,10)), including an identical telomeric repeat (5′-TTAGGG-3′) that

*To whom correspondence should be addressed. Tel: +972 2 658 4902; Fax: +972 2 658 6975; Email: tzfati@mail.huji.ac.il
Correspondence may also be addressed to Joseph Shlomai. Tel: +972 2 675 8089; Fax: +972 2 675 7425; Email: josephs@ekmd.huji.ac.il
†The authors wish it to be known that, in their opinion, the first two authors should be regarded as joint First Authors.
Present address: Galina Glousker, Swiss Institute for Experimental Cancer Research (ISREC), School of Life Sciences, Ecole Polytechnique Fédérale de Lausanne (EPFL), 1015 Lausanne, Switzerland.

was suggested to be the primordial telomeric sequence (11), the formation of a t-loop structure (12) and the localization to the nuclear periphery (13). The subtelomeric regions in *Trypanosoma brucei* chromosomes include the variant surface glycoprotein (VSG) encoding genes. VSGs are surface antigens, which enable the bloodstream form of the parasite to evade the immune system of the host by switching monoallelic expression of an individual VSG from one subtelomeric expression site to another. The mechanism of antigenic variation has been studied extensively and the telomere length, structure and tethering to the nuclear periphery were implicated in the silencing and switching between VSG genes. The contribution of DNA recombination-mediated events to VSG switching was also shown, where the same VSG expression site remains active but expresses a different VSG (reviewed in (9,14–18)). Two telomeric double-stranded DNA binding proteins, TbRAP1 and TbTRF, were shown to colocalize with *T. brucei* telomeres (19,20), and two *Leishmania amazonensis* proteins, LaRbp38 and LaRPA-1, were shown to bind telomeric DNA (21,22). Interestingly, LaRbp38 also localizes to the kinetoplast, the single mitochondrion of trypanosomatids (21). The *T. brucei* orthologue, TbRbp38 (also termed p38), was implicated in kinetoplast DNA (kDNA) replication (23).

kDNA consists, in different trypanosomatids species, of a few dozen maxicircles (20–40 kb) and a few thousand minicircles (0.5–10 kb), which are interlocked topologically into a DNA network. Minicircles in all the trypanosomatid species studied, contain a conserved dodecamer sequence, designated universal minicircle sequence (UMS), which has been mapped to the replication origin of the minicircles (reviewed in (24–28)). The G-rich strand of UMS is bound specifically by the UMS binding protein (UMSBP), a sequence-specific single-stranded DNA binding protein, which consists of five to nine CCHC-type zinc finger domains in the different trypanosomatids species. UMSBP has been first identified in *Crithidia fasciculata* and its binding to the minicircle replication origin has been extensively characterized (29–39). Genes encoding orthologous proteins have been identified in all other trypanosomatid species studied (40,41). Immunolocalization of UMSBP in *C. fasciculata* revealed two mitochondrial protein foci in the kinetoflagellar zone, near the suggested sites where minicircle replication initiates (29,42).

Two *UMSBP* paralogs were found in *T. brucei*, designated *TbUMSBP1* and *TbUMSBP2* (40). *TbUMSBP1* encodes for a 140 amino acid protein, containing 5 CCHC-type zinc finger domains, while *TbUMSBP2* encodes for a 213 amino acid protein containing 7 CCHC-type zinc fingers. Silencing of *TbUMSBP1* by RNA interference (RNAi) had no detectable effect on cell growth or morphology of its subcellular organelles, whereas silencing of *TbUMSBP2* resulted in accumulation of DNA in the nuclei, increase of the nuclei dimensions and accumulation of cells containing one kinetoplast and no nucleus (1K0N) (40). These cells, known as zoids (43), could be generated by cytokinesis of cells that have replicated their kDNA and nuclear DNA in the absence of nuclear mitosis, leading to loss of nuclei and cell growth arrest. These observations indicated that TbUMSBP2 plays a role in nuclear DNA metabolism. Based on the similarity between the telomeric 3′ overhang and the G-rich single-stranded UMS, we hypothesized that TbUMSBP2 binds the telomeric 3′ overhang and functions at telomeres. Here we demonstrate by fluorescence *in situ* hybridization (FISH) combined with immunofluorescence (IF), the colocalization of TbUMSBP2 with telomeres. We further show that depletion of TbUMSBP2 results in clustering of telomeres and activation of DDR, as indicated by phosphorylated histone H2A (γH2A) colocalizing mainly with the telomeres. While we could not detect a change in the overall telomere length within the short time frame of the knockdown experiment, we observed reduced G-rich telomeric overhang and increased amount of single-stranded C-rich telomeric repeats. In addition, in the TbUMSBP2-depleted cells we found increased levels of extrachromosomal telomeric (t)-circles, presumably generated by t-loop excision. These observations are typically associated with telomere deprotection and elevated recombination, and indicate that TbUMSBP2 binds to the G-rich telomeric overhang and plays an essential role in maintaining the stability and function of telomeres in *T. brucei*.

MATERIALS AND METHODS

Trypanosoma brucei cell culture and RNAi

The procyclic 29-13 cell line was cultured at 28°C in BECK's medium supplemented with 10% fetal bovine serum, 15 μg/ml G418 and 50 μg/ml hygromycin. RNAi was carried out as described previously (44,45). A 198-bp fragment of the Tb10.70.0820 (*TbUMSBP2*) gene was ligated into the stem-loop vector pLEW100, and the resulting plasmid was linearized and electroporated into the procyclic 29-13 cells. Twenty-four hours after electroporation, cells were selected under 2.5 μg/ml phleomycin. Selected transfectants were further cloned by limiting dilution in a 96-well plate. To induce RNAi, the clonal cell line was incubated with 1.0 μg/ml tetracycline and cell growth was monitored daily using a hemocytometer.

Purification of recombinant TbUMSBP2

Preparation of recombinant TbUMSBP2 was carried out following Sela and Shlomai (37). Briefly, TbUMSBP2 coding sequence was cloned into pHISParallel II expression vector and transformed into in *Escherichia coli* BL21. Protein expression was induced by 1 mM isopropyl-D-thiogalactopyranoside (IPTG) for 5 h at 37°C. Cells were harvested and resuspended in lysis buffer (50 mM potassium phosphate pH 8, 300 mM NaCl, 10 mM imidazole, 20 mM β-mercaptoethanol) and lysed by four cycles of maximum-power sonication bursts of 30 s each (Misonic Sonicator XL). Triton X-100 was added to a final concentration of 1%, followed by a 30-min centrifugation at 10 000 × *g* and 4°C. The supernatant was added to Ni-nitrilotriacetate (NTA) beads (Qiagen) and incubated with gentle agitation at 4°C for 2 h. The beads were washed once with 40 bed volumes of buffer I (50 mM potassium phosphate pH 8, 600 mM NaCl, 10 mM imidazole, 20 mM β-mercaptoethanol) followed by 10 bed volumes of wash buffer I with no NaCl added. Bound TbUMSBP2 was

eluted from the column using elution buffer (50 mM potassium phosphate, pH 8.0, 250 mM imidazole and 20 mM β-mercaptoethanol).

Electrophoretic mobility shift analysis (EMSA)

Analyses were carried out as described previously (32). The 10 or 20 μl reaction mixture contained 25 mM Tris–Cl, pH 7.5, 5 mM $MgCl_2$, 2 mM DTT, 10% glycerol, 1.25 mg/ml of bovine serum albumin (BSA) 50 μg/ml poly(dI-dC)·poly(dI-dC), 25 fmol 5′-^{32}P-labeled 18-mer telomeric repeat (5′-AGGGTT-3′)$_3$ and recombinant TbUMSBP2, as indicated. Reaction mixtures were incubated at 4°C for 15 min and electrophoresed in 8% native polyacrylamide gel (1:32 or 1:19) bisacrylamide/acrylamide) in TAE buffer (6.7 mM Tris-acetate, 3.3 mM sodium acetate, 1 mM Ethylenediaminetetraaceticacid (EDTA), pH 7.5). Electrophoresis was conducted at 4°C and 16 V/cm, for 75 min. Protein–DNA complexes were quantified by exposing the dried gels to an imaging plate and analyzing by PhosphorImager.

In situ tagging of TbUMSBP2

In situ tagging of *TbUMSBP2* with a triple hemagglutinin (3 × HA) tag in *T. brucei* was performed by homologous recombination as described previously (46). We used the pMOTag2H. Procyclic *T. brucei* cells were transfected using the Cytomix buffer (120 mM KCl, 0.15 mM $CaCl_2$, 10 mM potassium phosphate buffer pH 7.6, 25 mM Hepes pH 7.6, 2 mM EDTA pH 8.0, 5 mM $MgCl_2$, 100 μg/ml BSA, 2 mM EGTA pH 7.6). Electroporation was performed in a BTX electroporation system (BioRad). Bleomycine resistance was used to select for the integration of *HA-TbUMSBP2* and cells were cloned by limiting dilution. Transfectants of pMOTag2H were selected with 2.5 μg/ml bleomycine, and clones were isolated by limiting dilution.

Immunofluorescence microscopy

10^6 cells were washed once in 1 ml of phosphate-buffered saline (PBS) containing 1 mg/ml glucose, resuspended in 0.1 ml of PBS, diluted with an equal volume of ice-cold 6% paraformaldehyde in PBS and placed on ice for 15 min. Paraformaldehyde was inactivated by the addition of 1 ml of 0.1 M glycine in PBS, and cells were pelleted (5 min, 800 × *g*, at room temperature), washed with 1 ml of PBS, 0.1 M glycine and resuspended in 0.2 ml of PBS. Cells were applied to poly-L-lysine coated slides, allowed to adhere for 15–30 min, immersed in methanol (−20°C, 1 h), and rehydrated by three 5-min washes in TBST (50 mM Tris-Cl, pH 7.5, 150 mM NaCl, 0.1% Tween-20). When used for immunolocalization of TbUMSBP2, slides were treated with a primary anti-HA antibody (1:100 in 3% BSA, TBST) or affinity purified anti-TbUMSBP2 antibodies for 1 h. The samples were washed in TBST and exposed to a secondary Alexa Fluor 488 goat anti-mouse antibody (1:2000 in 3% BSA, TBST) for 1 h, washed in TBST, stained with mounting medium including DAPI (Sigma) and coverslips were sealed with clear nail polish. Fluorescence microscopy was conducted using a 100X objective lens on a Nikon E600 Upright microscope (Olympus Instruments) using ImagePro Plus software (Media Cybernetics) for image processing. For antibody affinity purification, purified recombinant TbUMSBP2 was immobilized on nitrocellulose membrane and incubated with rabbit anti- CfUMSBP serum. The membrane was washed with PBST (0.05% Tween-20 in PBS) and eluted with 100 mM glycine (pH 2.5). Resultant eluates were neutralized with 1M Tris pH 8.0 and dialyzed overnight against PBS.

Fluorescence *in situ* hybridization (FISH) and immunofluorescence combined with FISH

Cells were washed with PBS, mounted on poly-L-lysine-coated slides, fixed with 8% formaldehyde in PBS at room temperature for 20 min and then treated with 1% Triton X-100 for 5 min. Following wash with PBS, the cells were prehybridized in hybridization buffer [70% formamide, 2% BSA, 100 ng tRNA, 0.6 × saline sodium citrate (SSC) buffer pH 7.0 and 45 ng telomeric peptide nucleic acid (PNA) probe, Cy3-(CCCTAA)$_3$], for 5 min at 85°C in a humid chamber. After denaturation, hybridization was continued overnight, at room temperature in the dark. Slides were washed twice for 15 min with 70% (vol/vol) formamide, 10 mM Tris-Cl pH 7.2 and 0.1% BSA, and then three times for 5 min with 0.15 M NaCl, 0.1 M Tris-Cl pH 7.2 and 0.08% Tween-20. Nuclei were counterstained and mounted with Fluoroshield with DAPI (Sigma). Fluorescence microscopy was conducted as described above. When IF was combined with FISH, cells were first submitted to IF and subsequently to FISH.

Western analysis

For western blotting, whole cell lysates were subjected to sodium dodecyl sulphate-polyacrylamide gel electrophoresis (SDS-PAGE; 16.5% acrylamide) and electroblotting to Protran BA85 cellulose nitrate membrane (Schleicher & Schuell). A primary anti *T. brucei* γH2A and anti *C. fasciculata* UMSBP antibodies were used at 1:200 and 1:500 dilution, respectively, incubated for 1 h at room temperature, washed and incubated for 1 h with a secondary goat anti-rabbit IgG HRP at a 1:2000 dilution. Signals were detected using an ECL preparation as recommended by the manufacturer (Biological Industries) and quantified by MicroChemi (DNR Bio Imaging system).

Preparation of cytosolic and nuclear extracts

Trypanosoma brucei nuclei were purified as was previously described (47), except that cell lysis was conducted by nitrogen cavitation bomb. Nuclear extract was prepared by extraction with high salt concentration buffer (20 mM Tris–HCl, 420 mM NaCl, 1.5 mM $MgCl_2$, 0.2 mM EDTA, 1 mM Phenylmethylsulfonyl fluoride (PMSF) and 25% (v/v) glycerol, adjusted to pH 8.0). For cytosolic extract, 5×10^8 cells/ml were harvested by centrifugation and resuspended in a hypotonic buffer (20 mM Hepes pH 7.9, 20 mM KCl, 150 mM sucrose, 3 mM $MgCl_2$ and 1 mM DTT, 0.2% NP40, 1 mM PMSF) and passed through a 26-gauge needle. The extract was centrifuged and supernatant was assayed as cytosolic fraction.

Telomere disfunction induced foci (TIF) assay

TbUMSBP2 RNAi was performed as described above. 10^6 *T. brucei* cells, which were tetracycline-induced, were pelleted at day 3 post-induction. The cells were resuspended in 1% (vol/vol) formaldehyde in PBS and incubated at 4°C for 1 h. Cells were pelleted (at 5200 × *g*, for 1 min at 4°C), washed with chilled PBS, and then with 0.5 ml of 1% BSA in PBS. Cells were resuspended in PBS containing 1% BSA and applied to microscope slides for 3 h at room temperature. To permeabilize the cells, they were treated with 0.5% Triton-X-100 in PBS for 20 min. A primary rabbit-γH2A antibody was used at a 1:250 dilution in 3% fetal bovine serum (FBS) in PBS for 1 h and washed with PBS. A secondary Alexa Fluor 488 donkey anti-rabbit antibody was used at 1:500 dilution in in PBS containing 3% FBS for 1h and then washed in PBS. Cells were then submitted to the FISH procedure described above.

In-gel hybridization analysis of single-stranded telomeric DNA

In-gel hybridization was performed following (48). Genomic DNA samples (1–1.5 μg) were digested with restriction endonucleases HinfI or HinfI and AluI (NEB Inc.) and separated on a 0.7% agarose gel. The samples were run in duplicates for hybridization with C-rich and G-rich telomeric probes in parallel. Following electrophoresis, the gels were dried under vacuum for 1 h at room temperature, then for 1 h at 50°C, prehybridized for 1 h at 50°C in Church mix (0.5 M Na_2HPO_4 pH 7.2, 1 mM EDTA, 7% SDS) and hybridized overnight at 50°C with ^{32}P-5′-end-labeled $(AACCCT)_3$ and $(AGGGTT)_3$ probes separately. After hybridization, the gels were washed three times with 4 × SSC at room temperature and once with 4 × SSC at 40°C (30 min each wash), and exposed to film or PhosphorImager. Following hybridization, gels were denatured by incubation in 0.5 M NaOH and 1.5 M NaCl for 30 min, neutralized in 1.5 M NaCl and 0.5 M Tris–HCl pH 7.0 twice for 15 min, rinsed with H_2O, prehybridized, hybridized and washed as previously. To monitor the relative overhang signal, the signal intensity for each lane (in the area presumably corresponding to the telomeric fragments based on the denatured hybridization) was quantified from the images before and after denaturation using *Image J* (Rasband, W.S. (1997–2014), U.S. National Institutes of Health, Bethesda, MD, USA, http://imagej.nih.gov/ij/), the native signal was divided by the denatured signal and normalized to the uninduced control.

Two-dimensional gel electrophoresis

Two-dimensional (2D) gel electrophoresis was modified from (49). A total of 5 μg genomic DNA samples, either undigested or digested with HinfI, were electrophoresed on a 0.4% agarose gel (first dimension) at room temperature and 1V/cm for 16 h. The lanes were cut (removing the first 1 cm from the wells), embedded in a second dimension gel (1.2% agarose with 0.3 μg/ml ethidium bromide) and electrophoresed at 4.5V/cm for 6 h. The gel was dried, cut to separate the duplicated samples and hybridized side by side with C- and G-probes to detect single-stranded telomeric DNA, as described for in-gel analysis. After exposure, the gels were denatured and hybridized again with the same probes to detect the total telomeric DNA. Supercoiled DNA ladder (NEB Inc), containing nine supercoiled plasmids (2–10 kb), was used as reference.

C-circle and G-circle assays

C-circle assay was performed as described in (50). Briefly, 300 ng of genomic DNA was digested with HinfI (NEB Inc.) for 1 h at 37°C. Duplicated samples were undigested or digested with 10 units of exonuclease V (Exo V) in the buffer supplemented with 1 mM adenosine triphosphate (ATP), as recommended by manufacturer (NEB Inc), for 1 h at 37°C. For C-circle detection, the ϕ29 DNA polymerase reactions contained the digested genomic DNA as indicated, 0.2 mg/ml BSA, 0.1% Tween-20, 1 mM each of dATP, dGTP and dTTP (or only dATP and dTTP), 1 x ϕ29 buffer and 7.5 U ϕ29 DNA polymerase (NEB Inc.) or no ϕ29 DNA polymerase as control. The reactions were incubated overnight at 30°C, and then the ϕ29 DNA polymerase was inactivated by incubation at 65°C for 20 min. Genomic DNA from U2OS ALT cells and immortalized human fibroblasts were used as positive and negative controls, respectively. The reaction products were run on 0.6% agarose gel in 0.5 × TBE, the gel was dried and hybridized with a 5′ end-labeled $(AACCCT)_3$ oligonucleotide probe, as described under 'in-gel hybridization analysis'. G-circle assay was performed in a similar manner, except for using dATP, dCTP and dTTP (or only dATP and dTTP) in the ϕ29 polymerase reaction and 5′ end-labeled $(AGGGTT)_3$ hybridization probe.

RESULTS

TbUMSBP2 colocalizes with telomeres in the nucleus

Silencing of *TbUMSBP2* had severe effects on the nuclear genome and its segregation (40), yet the nuclear target of this protein has not been described. Earlier immunostaining analysis of wild-type (WT) *T. brucei*, using antibodies raised in mice against *C. fasciculata* UMSBP and shown by western analysis to detect both TbUMSBP1 and TbUMSBP2, failed to detect a nuclear signal (40). To re-examine the specific subcellular localization of TbUMSBP2, we used *T. brucei* cells expressing HA-tagged TbUMSBP2 from its endogenous promoter and genomic locus (Supplementary Figure S1). IF using anti-HA antibodies clearly demonstrated the nuclear localization of TbUMSBP2 (Figure 1A). To ensure that the tagging of TbUMSBP2 did not affect its subcellular localization, we re-analyzed WT *T. brucei* cell by IF, using antibodies raised in rabbits against CfUMSBP and affinity-purified against recombinant TbUMSBP2. This IF analysis again localized TbUMSBP2 to the nucleus (Figure 1B), confirming the results obtained with the HA-tagged TbUMSBP2. These observations were further supported by fractionation of *T. brucei* cells followed by western analysis using the affinity-purified anti TbUMSBP2 antibodies, showing the presence of TbUMSBP2 in the nuclear

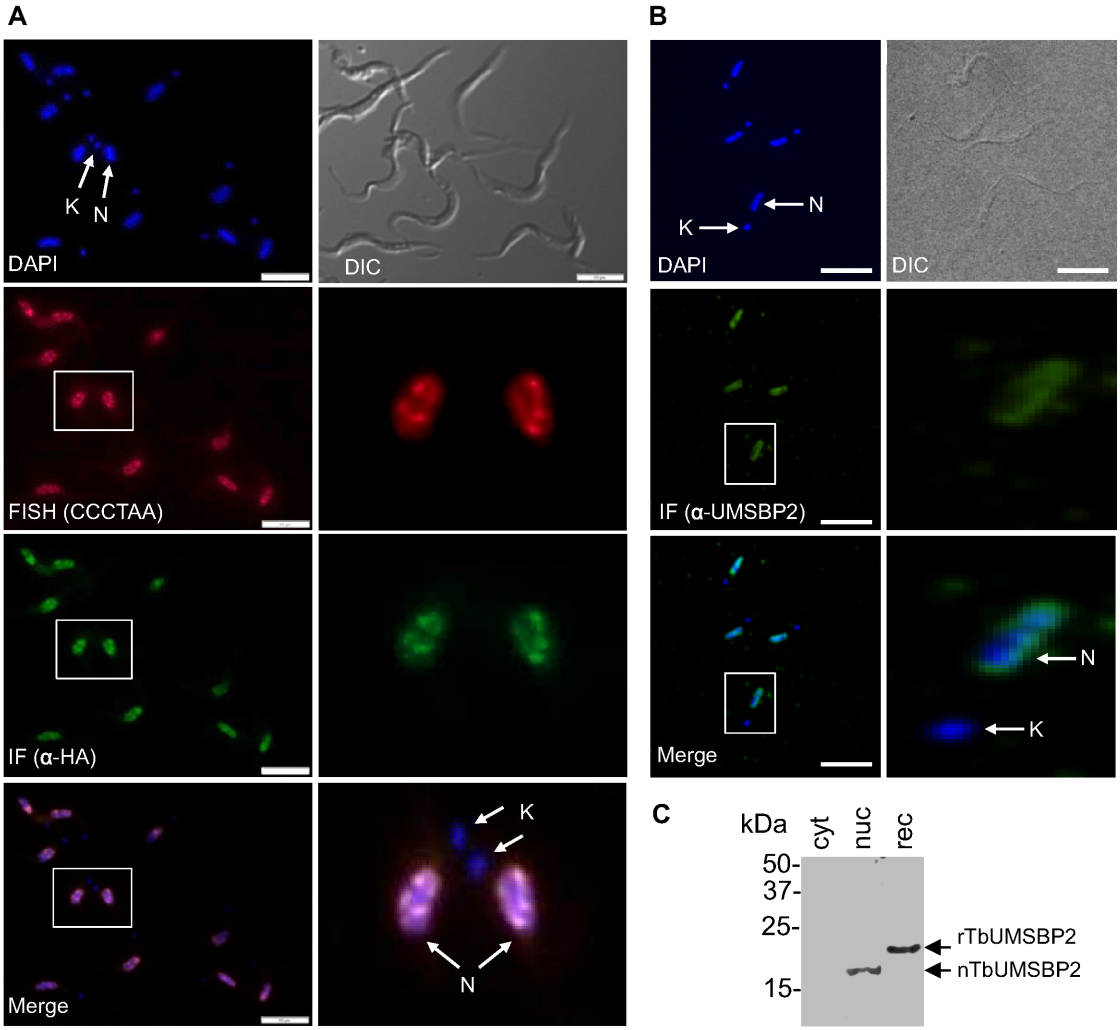

Figure 1. TbUMSBP2 colocalizes with telomeres in *Trypanosoma brucei.* (**A**) Combined IF and FISH analysis: DAPI staining (blue) shows the nucleus (N) and the kinetoplast (K); FISH using a telomeric PNA-Cy3-$(CCCTAA)_3$ probe (red) labels the telomeric repeats; and IF using anti HA antibodies (green) detects the HA-tagged TbUMSBP2. Merge is of the blue, green and red. DIC indicates differential interference contrast. Magnified images (5-fold) of two nuclei are shown on the right. Scale bars, 10 μm. (**B**) IF of TbUMSBP2 in WT *T. brucei* (green) was conducted using affinity purified anti TbUMSBP2 antibodies. Merge is of the blue and green. Magnified images (8-fold) of a nucleus are shown on the right. Scale bars, 10 μm. (**C**) A total of 50 μg of cytosolic (cyt) and nuclear (nuc) fractions of WT *T. brucei* cells were subjected to western blot analysis using affinity purified anti-TbUMSBP2 antibodies. His tagged recombinant TbUMSBP2 (rTbUMSBP2) was used as positive control. nTbUMSBP2, nuclear TbUMSBP2.

fraction (Figure 1C). Altogether, while the crude mouse anti-CfUMSBP antibodies used earlier detected only mitochondrial signal, apparently corresponding to TbUMSBP1, the more specific anti-HA and affinity-purified rabbit anti-TbUMSBP2 antibodies enabled the specific detection of TbUMSBP2 in the nucleus.

Given the similarity between UMS and the telomeric sequence, we combined IF with FISH using a telomeric probe, to test whether TbUMSBP2 is a telomeric protein (Figure 1A). DAPI-staining marks the nucleus and the kinetoplast (N and K), and differential interference contrast (DIC) provided a whole cell image of the parasites. FISH analysis demonstrated the expected intranuclear localization of *T. brucei* telomeres (9,15,51). IF localized TbUMSBP2 to the nucleus as well, where, as demonstrated by the merging of the DAPI, FISH and IF staining, it colocalized precisely with the telomeres.

TbUMSBP2 binds specifically to the telomeric G-strand sequence *in vitro*

Considering the high sequence similarity of the mitochondrial UMS (5′-GGGGTTGGTGTA-3′, underlined residues) and two telomeric repeats (5′-AGGGTTAGGGTT-3′), we explored the possibility that the G-rich telomeric overhang serves as the nuclear binding site for TbUMSBP2. First, we examined the binding of purified recombinant TbUMSBP2 (Figure 2A) to the telomeric sequence *in vitro,* by electrophoretic mobility shift assay (EMSA; Figure 2B). Three radioactively-labeled oligonucleotide ligands were used, each containing three telomeric repeats: the single-stranded C-rich strand $(AACCCT)_3$, its complementary single-stranded G-rich strand $(AGGGTT)_3$ and the double-stranded form of these two oligonucleotides. As shown in Figure 2B, TbUMSBP2

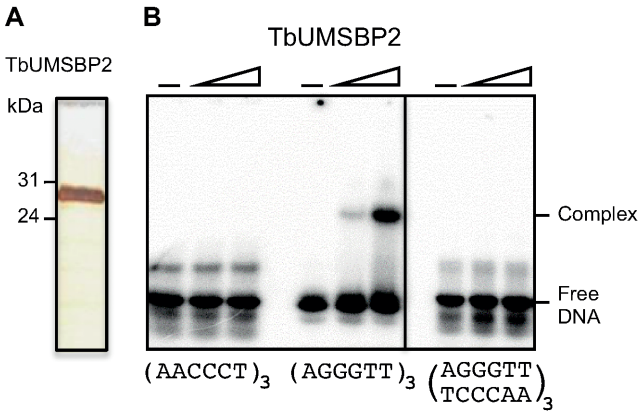

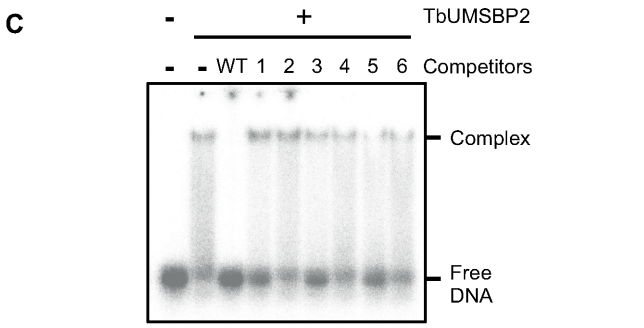

D

Competitor	Sequence (1 6 12 18)	UMSBP2-DNA complex (%)
–		100
WT	AGGGTTAGGGTTAGGGTT	1
T1	GGGGTTAGGGTTAGGGCC	55
T2	AAAATTAGGGTTAGGGTT	83
T3	AGGGCCGGGGTTAGGGTT	32
T4	AGGGTTAAAATTAGGGTT	58
T5	AGGGTTAGGGCCGGGTT	19
T6	AGGGTTAGGGTTAAATT	58

Figure 2. TbUMSBP2 binds the G-rich telomeric repeats. (**A**) Recombinant His-tagged TbUMSBP2 was expressed, purified to apparent homogeneity and analyzed by SDS-PAGE followed by silver staining. (**B**) The binding of TbUMSBP2 (12.5 and 125 fmol) to 5′-^{32}P-labeled DNA oligonucleotides (25 fmol): single-stranded stranded $(AACCCT)_3$; single-stranded $(AGGGTT)_3$; and double-stranded conformation $[(AGGGTT)_3{\cdot}(TCCCAA)_3]$ was monitored by EMSA. (**C**) Binding competition analysis using 25 fmol of 5′-^{32}P-labeled $(AGGGTT)_3$ probe and 125 fmol of TbUMSBP2 in the absence or presence of 10-fold molar excess of unlabeled $(AGGGTT)_3$ (WT) oligonucleotide or one of six mutants each containing a tri-nucleotide transition substitution (T1-T6, panel D). (**D**) The relative amounts of protein–DNA complex formed with the radioactive probe in the presence of each unlabeled competitor were quantified and normalized to the binding in the absence of competitor.

binds only the telomere single-stranded G-strand. No nucleoprotein complex was detected with either the C-strand or the double-stranded form. These observations indicated that TbUMSBP2 could potentially bind the G-rich single-stranded telomeric sequence at the 3′ overhang or an internal single stranded sequence, which can be displaced by the overhang while forming the t-loop. To assess the sequence specificity of the interaction of TbUMSBP2 with the telomeric G-strand, a binding competition analysis was performed by EMSA, using a series of G-strand-derived unlabeled 18-mer competitors, each containing three successive transition mutations (Figure 2C and D). This analysis revealed that each of the mutations reduced the capacity of the unlabeled oligonucleotides to compete with the WT probe on the binding of TbUMSBP2. Transition substitution of the three G residues at position 2–4 (T2) had the most dramatic effect (83.3% of the labeled WT probe remaining bound, as compared to ∼1% remaining in the presence of unlabeled WT competitor). Transition substitution of the three G residues at position 8–10 (T4) or 14–16 (T6) had an intermediate effect (58% of the labeled WT probe remaining bound). At last, mutation introduced at the two TTA sequences at positions 5–7 (T3) and 11–13 (T5), had a milder effect (32 and 19%, respectively). This analysis revealed the sequence-specificity of the interaction between TbUMSBP2 and the telomeric G-strand, as has been previously reported for the CfUMSBP-UMS interaction (35). Based on its colocalization with telomeres in the nucleus and its specific binding characteristics we suggest that TbUMSBP2 localizes to telomeres and binds the telomeric 3′ overhang or internally displaced G-rich single-stranded telomeric sequences.

TbUMSBP2 plays a role in telomeres protection and their nuclear localization

The *Caenorhabditis elegans* single-stranded telomeric binding protein POT-1 anchors telomeres to the nuclear periphery through its interaction with the nuclear envelope protein SUN-1 (3). To study if TbUMSBP2 has a similar function, we examined the effects of TbUMSBP2 depletion (40) on the nuclear localization of the telomeres. Interestingly, upon tetracycline-induced RNAi and knockdown of *TbUMSBP2*, the *T. brucei* telomeres clustered together, generating a spectrum of phenotypes of cells that have single or few telomere foci in the nucleoplasm (Figure 3, +Tet). These results suggest that the interaction of TbUMSBP2 with telomeres is important for their position and distribution at the nucleus. However, the observed change of telomere positioning may also be due to cell-cycle arrest and the increased fraction of G2/M cells, as observed by FACS (Supplementary Figure S2).

Next, we asked whether TbUMSBP2 functions in the repression of DDR at the chromosome ends, such as the role played by the mammalian telomeric ssDNA binding protein POT1 (5). Depletion of POT1 resulted in the activation of DDR at telomeres and the formation of telomere dysfunction-induced foci (TIFs). These foci, visualized in mammalian cells by the colocalization of DDR fac-

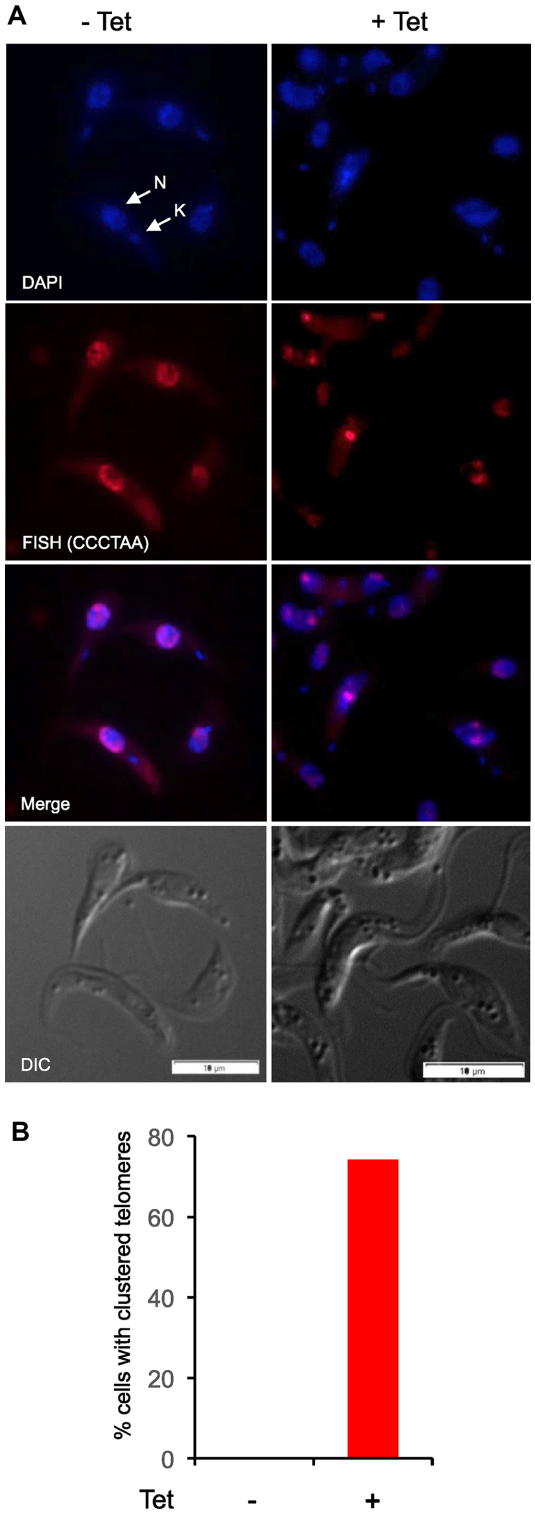

Figure 3. Knockdown of *TbUMSBP2* results in de-localization of telomeres. (**A**) FISH analysis of uninduced cells (−Tet) and cells at day 3 post *TbUMSBP2* RNAi induction (+Tet): DAPI staining of the nucleus (N) and kinetoplast (K) is in blue and FISH detection of telomeres using telomeric PNA-Cy3-$(CCCTAA)_3$ probe in red. Merge shows the blue and red together. Differential interference contrast (DIC) shows the *Trypanosoma brucei* cells. Scale bar, 10 μm. (**B**) Quantification of uninduced (−) and induced (+) cells (n = 100 and 68 cells, respectively), containing telomeres clustered in 1–3 foci in the nucleus.

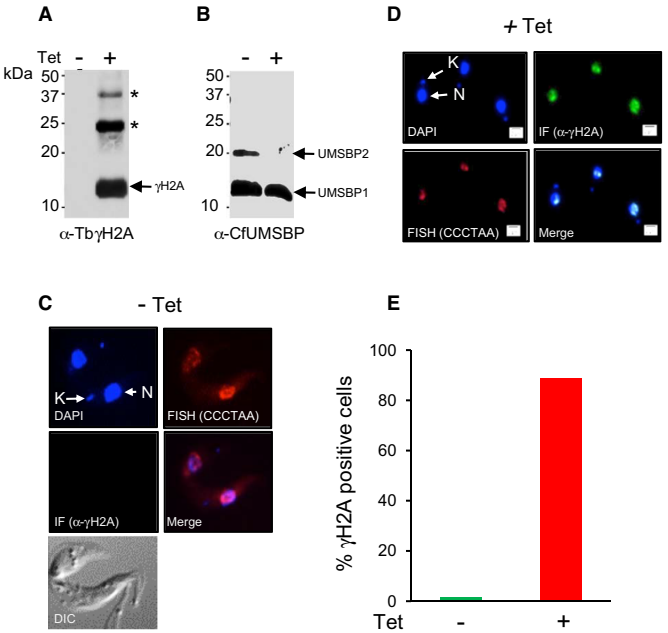

Figure 4. *TbUMSBP2* knockdown induced DDR at telomeres. Western blot analysis of *TbUMSBP2* RNAi induced (+) and uninduced (−) cells was conducted as described under 'Materials and Methods' section, using anti γH2A (**A**) and CfUMSBP (**B**) antibodies. RNAi induction was performed for 3 days. Immunoreactive bands that appeared in the blots are marked: γH2A, UMSBP1, UMSBP2; asterisk, ubiquitinated form of γH2A. Telomere dysfunction-induced foci (TIF) assay in uninduced (**C**) and RNAi-induced (**D**) *Trypanosoma brucei* cells. Shown are DAPI staining of the nucleus (N) and kinetoplast (K), IF using anti γH2A antibodies, FISH using a telomeric PNA-Cy3-$(CCCTAA)_3$ probe and merging of the DAPI, IF and FISH images. Scale bar, 2 μm. (**E**) Quantification of nuclei stained by anti γH2A antibodies in uninduced and induced cells (n = 108 and 44 cells, respectively).

tors such as phosphorylated histone H2AX (γH2AX) with telomeres, are a hallmark of telomere dysfunction. In trypanosomes, phosphorylation of the histone H2A to γH2A was observed upon induced DNA damage (52,53). We first examined extract prepared from *TbUMSBP2* knockdown cells for the presence of γH2A by western blot analysis using anti-γH2A antibodies (Figure 4A). No γH2A could be detected in normal (−Tet) cells, whereas *TbUMSBP2* knockdown (+Tet) cells induced the phosphorylation of histone H2A (Figure 4A). Moreover, these analyses revealed the generation of slower migrating protein bands adding 8.6 and 17.2 kDa to γH2A, which are consistent with mono- and di-ubiquitinated species of the γH2A (Figure 4A, asterisks), as has been previously describe to occur in response to DNA damage (54–57). Western blot analysis using anti-CfUMSBP antibodies, which interact with both TbUMSBP1 and TbUMSBP2, revealed that silencing of the *TbUMSBP2* gene suppressed its expression, but not that of *TbUMSBP1*, attesting for the specific targeting of *TbUMSBP2* (Figure 4B).

Next, we examined the cells for the formation of TIFs by immunostaining for γH2A combined with telomere FISH. No γH2A signal could be detected in the uninduced cells (Figure 4C and E), but upon *TbUMSBP2* knockdown γH2A is clearly detected, mostly in one or a few foci

colocalizing with the telomeres (Figure 4D and E). Weaker γH2A staining is observed also outside these brighter foci, indicating that some telomeres remain outside of the main foci or that DNA damage occurs also at non-telomeric sites. Nevertheless, the stronger signal colocalizing with telomeres suggests that TbUMSBP2 is essential for the repression of DDR at telomeres, the major function of telomeres.

Trypanosoma brucei cells contain linear and circular extra-chromosomal telomeric repeats with single-stranded regions

Single-stranded telomeric binding proteins regulate polymerization and nuclease activities determining the length of the telomeric 3′ overhang; depletion of human POT1 shortened the G-rich 3′ overhang (5), while mutations in the CST complex resulted in elongation of the overhang sequence (58–60). To examine the effect of TbUMSBP2 depletion on the telomeric overhang, we used in-gel hybridization to detect G- and C-strand overhangs using radioactively-labeled C-rich $(AACCCT)_3$ and G-rich $(AGGGTT)_3$ probes, respectively. First we hybridized the gel under non-denaturing conditions to detect single-stranded telomeric DNA, and then we denatured the DNA *in situ* and re-hybridized to the same probes (Figure 5). We were able to detect G-rich single-stranded telomeric repeats, which largely diminished upon pre-incubation with Exo I (3′ to 5′ exonuclease; Supplementary Figure S3), indicating that they have single stranded 3′ ends. Interestingly, we also detected C-rich single-stranded telomeric repeats, which largely diminished upon pre-incubation with RecJF (5′ to 3′ exonuclease; Supplementary Figure S4), indicating that they have single stranded 5′ ends. However, in addition to the main hybridization bands observed under both native and denaturing conditions, native hybridization with both probes revealed a smear of fragments with heterogeneous length. This suggested the presence of a population of chromosomal or extra-chromosomal telomeric repeats (ECTRs) with a larger fraction of single-stranded DNA than in the main bands (Figure 5; Supplementary Figures S3 and S4). To further examine the population of ECTRs, we employed neutral-neutral 2D gel electrophoresis, separating first on the basis of DNA size and then according to its conformation (Figure 6). We electrophoresed side by side a duplicated sample of undigested WT *T. brucei* genomic DNA and hybridized the native DNA in gel with a C-rich or a G-rich telomeric probe (Figure 6A and B). In addition, we added to the sample circular, double-stranded linear and single-stranded linear DNA markers that were visualized by ethidium bromide staining (Figure 6C and Supplementary Figure S5). While the bulk of chromosomal DNA was omitted from the gel after the first dimension, we observed a significant amount of ECTRs, circular, linear and single-stranded, which hybridized to the probes under native conditions, thus containing single stranded regions (Figure 6). Such ECTRs may have obscured the chromosomal telomeric overhangs when assayed by 1D electrophoresis and in-gel hybridization in previous experiments (e.g. (61)) a difficulty that was solved by separating undigested chromosomal DNA by rotating agarose gel electrophoresis (RAGE) (18).

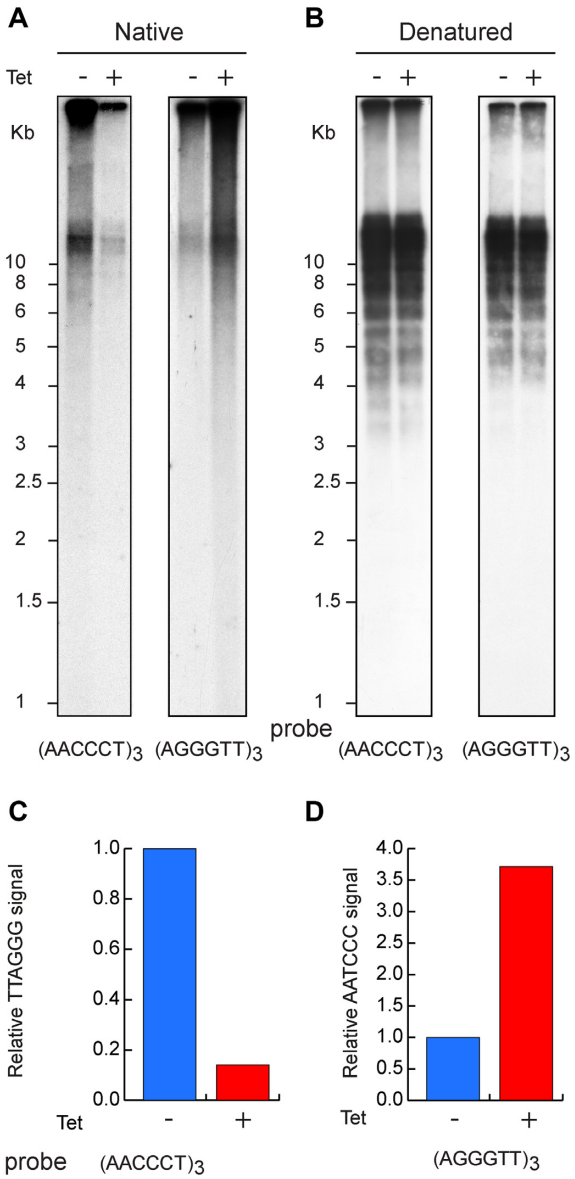

Figure 5. TbUMSBP2 knockdown altered the amount of single stranded telomeric DNA. DNA samples (1 μg) of uninduced cells (−) and cells at day 3 post *TbUMSBP2* RNAi induction (+), were digested with HinfI and AluI restriction endonucleases and analyzed by in-gel hybridization to C-probe $(AACCCT)_3$ or G-probe $(AGGGTT)_3$, first under native conditions (**A**) and then re-hybridized again to the same probes after denaturation (**B**), as described under 'Materials and Methods'. (**C** and **D**) the histograms represent the relative amounts of native signal (corresponding to single-stranded telomeric DNA) normalized to the denatured (total) signals. The uninduced control samples were set as 1.

TbUMSBP2 is required for the integrity of the telomere end

The overall telomere length was unchanged upon TbUMSBP2 knockdown, during the short course of the experiment (Figure 5B). However, the signal corresponding to the single-stranded G-rich telomeric sequences decreased to about 15% of the control sample, suggesting a significant shortening of the G-rich overhang [Figure 5, $(AACCCT)_3$ probe]. Interestingly, the signal corresponding to single-stranded C-rich telomeric sequences

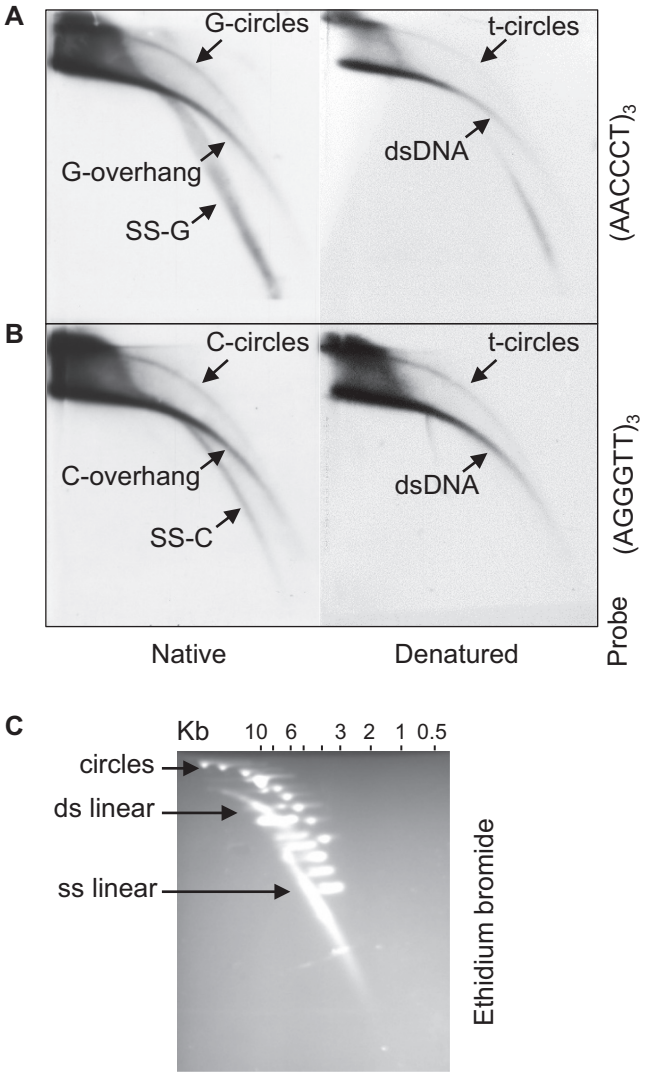

Figure 6. *Trypanosoma brucei* cells contain ECTRs. Undigested genomic DNA (5 μg) from WT (uninduced) cells was subjected to neutral-neutral 2D-gel electrophoresis in duplicates and dried. One gel (**A**) was hybridized with a radioactively labeled C-probe $(AACCCT)_3$, and the other (**B**) was hybridized with a G-probe $(AGGGTT)_3$, first under native conditions to detect single-stranded G-rich and C-rich telomeric repeats, respectively. Then, the DNA in the gels was denatured and re-hybridized to the same probes to detect both single- and double-stranded telomeric repeats. Indicated are single-stranded G- and C-rich telomeric sequences associated with linear dsDNA (G- and C-overhangs) and t-circles (G- and C-circles), and ssDNA (SS-G and SS-C). Note that after denaturation the hybridization signal was stronger, thus much shorter exposure was sufficient to visualize the dsDNA and thus ssDNA appears weaker or disappeared. (**C**) Ethidium bromide staining of the gel in (A) shows circular and linear dsDNA markers. Nicked circular DNA (circles) was generated by UV irradiation of supercoiled ladder, and single-stranded DNA (ss linear) was generated by UV irradiation followed by heat denaturation and snap cooling.

increased significantly upon TbUMSBP2 knockdown up to ∼370% relative to the control sample [Figure 5, $(AGGGTT)_3$ probe]. C-rich 5′ telomeric overhangs were detected in *C. elegans* and mammalian cells, in association with recombination-dependent telomere maintenance or rapid telomere deletion (62,63). The changes in the ratio of signals corresponding to G- and C-rich telomeric sequences as the result of TbUMSBP2 depletion (Figure 5; Supplementary Figures S3 and S4) indicate that TbUMSBP2 plays a role in telomere end maintenance and protection.

Disruption of *C. elegans* CeOB2/POT-2 was associated with increased formation of double-stranded extrachromosomal telomere (t)-circles and induced telomeric recombination (64). In mammalian cells, telomere maintenance by the recombination-dependent alternative lengthening of telomeres (ALT) mechanism, or expression of a dominant negative mutant of the telomeric protein TRF2, were associated with increased levels of C-rich overhangs and t-circles generated by t-loop excision (50,62,63). To examine the formation of t-circles with (or without) single-stranded regions, we employed 2D gel electrophoresis combined with in-gel hybridization to native DNA. Equal amounts of duplicated DNA samples from normal (−Tet) and TbUMSBP2-knockdown (+Tet) cells were electrophoresed in the same gel and hybridized side by side; one pair was hybridized to a C-rich probe and another to a G-rich probe (Figure 7). Consistent with the 1D in-gel hybridization (Figure 5), TbUMSBP2 knockdown reduced the signal corresponding to telomeric G-rich single-stranded DNA (Figure 7A, G-overhangs and SS-G). This signal was sensitive to exonuclease I, confirming the presence of G-rich 3′ overhangs (Supplementary Figure S5). Also consistent with the 1D in-gel hybridization, TbUMSBP2 knockdown increased the signal corresponding to telomeric fragments with C-overhangs and C-rich single-stranded DNA (Figure 7A, C-overhangs and SS-C). At last, TbUMSBP2 knockdown increased the formation of t-circles containing single stranded C-rich regions, and thus gaps in the G-strand. This subset of t-circles are termed here C-circles (Figure 7A, $(AGGGTT)_3$ probe). Following the native hybridization, the DNA was denatured in-gel and hybridized again with the same probes, revealing comparable amounts of linear telomeric dsDNA (Figure 7B and C). In addition, both probes revealed an increase in the arc corresponding to t-circles upon TbUMSBP2 knockdown (Figure 7B, t-circles). To confirm the detection of circular DNA, we pretreated a DNA sample from normal uninduced cells (−Tet) with exonuclease V, which degrades linear DNA. While t-circles were barely detected in the normal uninduced cells without exonuclease V treatment, they were well detected when most of the linear DNA was degraded and exposure was increased (Compare Figure 7B, −Tet $(AGGGTT)_3$ probe, with Supplementary Figure S6).

To further study the formation of telomeric circles we used ϕ29 DNA polymerase (50). This sensitive assay is based on the ability of ϕ29 polymerase to use a DNA circle with one intact strand and nicked or gapped complementary strand as a template for rolling-circle amplification, generating long multimeric ssDNA products. These products do not migrate out of the wells of a native agarose gel and can be detected by in-gel hybridization with a telomeric probe. Circles with intact C-strand and gapped or nicked G-strand, termed C-circles, produce G-rich products in a dGTP-dependent manner and are detected with a C-rich probe (Figure 8A). Circles with intact G-strand and gapped or nicked C-strand, termed G-circles, produce C-rich products in a dCTP-dependent manner and are detected with a G-rich probe (Figure 8B). The levels of C- and G-circles

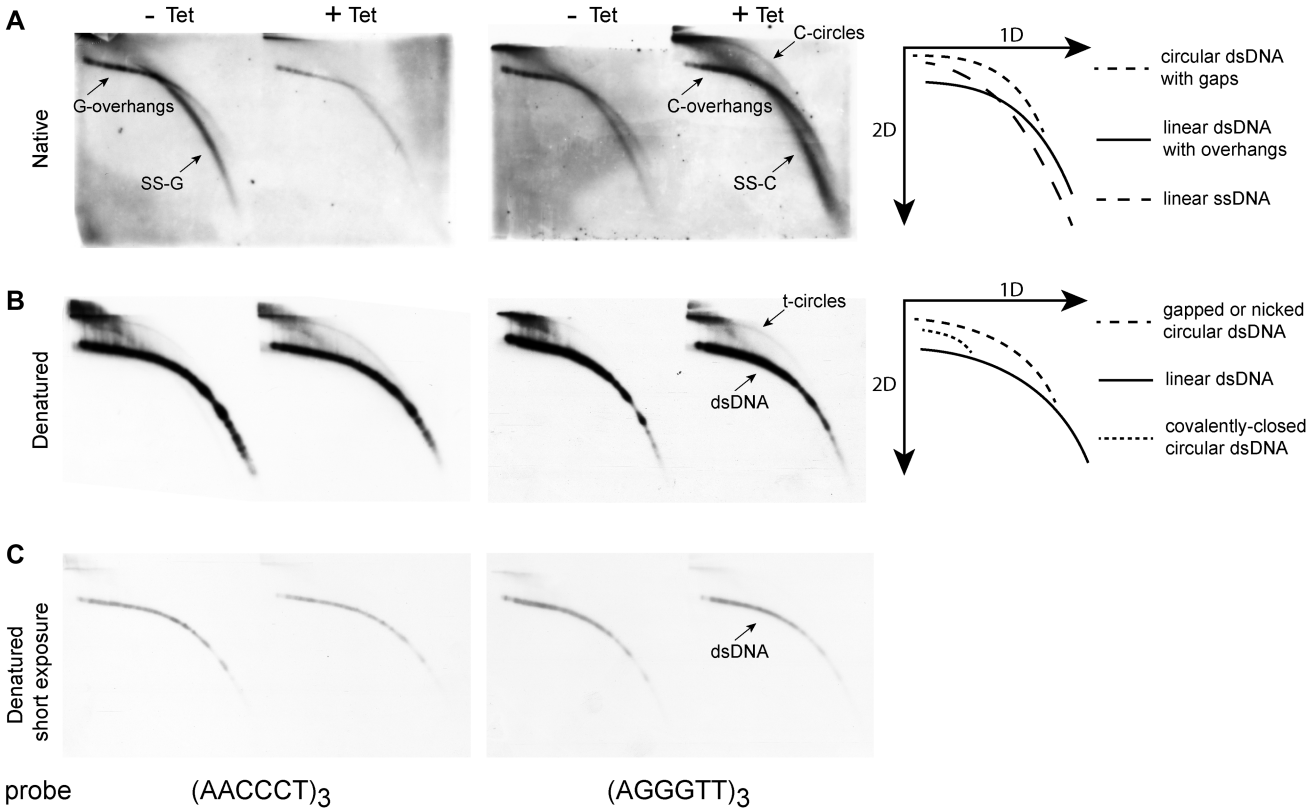

Figure 7. *TbUMSBP2* knockdown decreased G-overhangs and increased C-overhangs and telomeric circles. Equal amounts of DNA samples (5 μg), prepared from uninduced cells (−Tet) and cells at 3 days post *TbUMSBP2* RNAi induction (+Tet), were digested with HinfI and analyzed in duplicates by neutral-neutral 2D gel electrophoresis. (**A**) The gels were dried and hybridized in-gel under native assay conditions with a radioactively labeled C-probe, $(AACCCT)_3$, or G-probe, $(AGGGTT)_3$, to detect single-stranded G-rich or C-rich telomeric repeats, respectively. (**B**) The DNA was subsequently denatured *in situ* and re-hybridized to the same probes to detect both single- and double-stranded telomeric repeats. Note that after denaturation the hybridization signal was stronger; much shorter exposure was sufficient to visualize the dsDNA and thus ssDNA appears weaker or disappeared. (**C**) A shorter exposure of the gels in (B), showing comparable amounts of telomeric DNA. Schemes on the right illustrate the different arches of telomeric DNA observed by hybridization to native or denatured DNA, following (62,63). Indicated are G- and C- overhangs associated with linear dsDNA, ssDNA (SS-G and SS-C), telomere circles (t-circles) and a subset of t-circles containing gaps in the G-strand and single stranded regions of the C-strand (termed here as C-circles).

measured upon induction of TbUMSBP2 knockdown were about 12.0 and 8.8-fold higher than the levels in normal uninduced cells (Figure 8A and B), consistent with the results of the 2D electrophoresis (Figure 7). Both circle types were resistant to exonuclease V, which degrades the linear chromosomal telomeres that appear after denaturation and re-hybridization of the same gel (Figure 8 and Supplementary Figure S7). We used a human telomerase-negative cell line that maintains its telomeres by the ALT mechanism, which is known to be associated with high levels of C-circles (50), as a positive control, and telomerase positive human fibroblasts as a negative control (U2OS and fib-TERT in Supplementary Figure S8). As expected, U2OS cells displayed high levels of C-circles (panel A) and lower levels of G-circles (panel B), while no such circles were detected in the human fibroblasts under the assay conditions. Interestingly, uninduced *T. brucei* DNA contained both circles at higher levels than U2OS (about 7- and 25-fold higher than the levels in U2OS, per ng DNA, for C- and G-circles, respectively), suggesting that ongoing t-loop excision and t-circle formation occurs also in normal cells (Supplementary Figure S8). The levels of circles increased upon induction of *TbUMSBP2* knockdown to about 20- and 100-fold higher than the levels in U2OS, per ng DNA, for C- and G-circles, respectively (Supplementary Figure S8). However, since the *T. brucei* genome is about 100-fold smaller and contains more chromosomes, we normalized the amount of C- and G-circles to the total telomeric DNA, as quantified from the denatured and re-hybridized gel (Supplementary Figure S8C). These normalized values of C-circles are 0.2 and 0.6 of the level in U2OS, for the 3 ng uninduced and knockdown samples, respectively. Since the level of G-circles is lower in U2OS, the normalized values for G-circles are 2.2 and 6.4 for the 3 ng uninduced and knockdown samples, respectively. Altogether, our results indicate that TbUMSBP2 depletion disrupted the telomeres' ability to restrain t-loop excision and formation of extrachromosomal t-circles. The level of C-circles upon TbUMSBP knockdown is comparable to that in ALT cells. However, unlike in ALT cells, both C- and G-circles are equally elevated.

DISCUSSION

We have previously reported the harmful effect of TbUMSBP2 depletion on nuclear DNA metabolism,

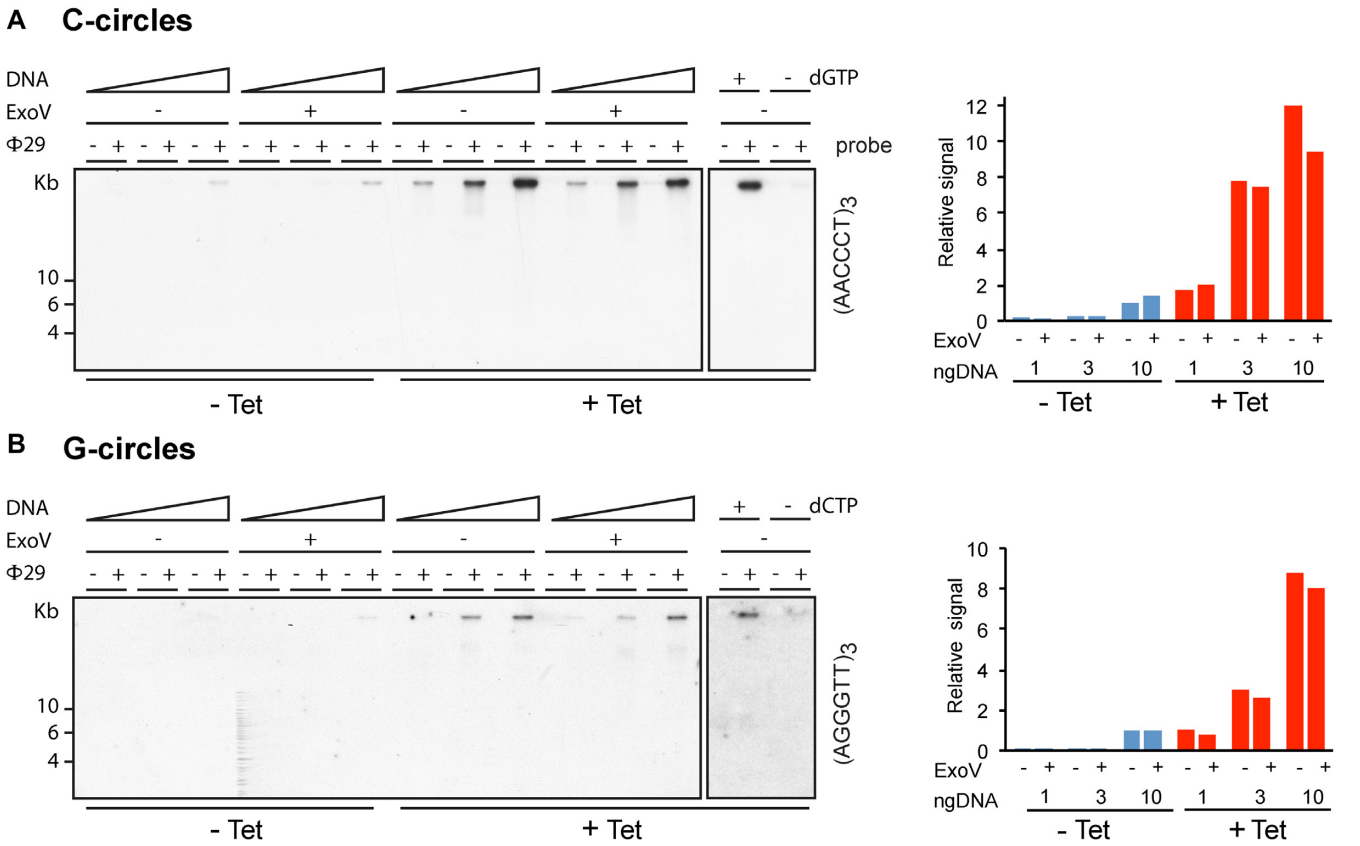

Figure 8. *TbUMSBP2* knockdown increased the levels of telomeric circles. Genomic DNA samples (1, 3 and 10 ng, indicated by a triangle above the lanes) extracted from uninduced cells (−Tet) and cells 3 days post *TbUMSBP2* RNAi induction (+Tet), were digested with exonuclease V (Exo V) or undigested, as indicated, and then assayed for the presence of (A) C-circles (t-circles containing intact C-strand and gapped or nicked G-strand) and (**B**) G-circles (t-circles containing intact G-strand and gapped or nicked C-strand) by ϕ29 DNA polymerase-dependent rolling circle amplification. Reaction products were electrophoresed, subjected to in-gel hybridization of native DNA with radioactively labeled C- or G-probe, as indicated to the right of the gel images. As controls, dGTP and dCTP were omitted from the C- and G-circles assays, respectively (right panels). Supplementary Figure S7 shows the same gels after denaturation and re-hybridization to the same probes to confirm the amounts of double-stranded telomeric DNA and its sensitivity to Exo V. The histograms on the right represent the native signals normalized to the signal of the 10 ng uninduced samples (−Tet) not digested with Exo V. Blue bar indicates the relative signal for the uninduced cells (−Tet) and red bars indicate the RNAi induced cells (+Tet).

which ultimately leads to cell growth arrest (40). These effects were unexplained since we could not detect TbUMSBP2 in the nucleus with the crude anti-CfUMSBP antibodies available at the time. In the current study, we examined the hypothesis that the conserved sequence of the telomere repeats, which is similar to UMS, serves as the nuclear binding target of TbUMSBP2. Indeed, we found that TbUMSBP2 is a telomeric protein that is essential for maintaining the telomere structure and function, explaining the harmful effects of its depletion. TbUMSBP2 colocalizes with telomeres at the nuclear periphery and binds *in vitro* to the single-stranded G-rich telomeric sequence (Figures 1 and 2), which is naturally found in the telomeric 3′ overhangs and in the displaced G-strand of the telomere (t)-loop. Depletion of TbUMSBP2 affected the intranuclear localization of the telomeres and induced DDR (Figures 3 and 4). Moreover, silencing of *TbUMSBP2* resulted in reduced G-rich 3′ overhangs and increased C-rich 5′ overhangs and extrachromosomal linear and circular telomeric sequences (Figures 5, 7 and 8), indicating that TbUMSBP2 is essential for telomere protection from degradation and recombinational processes.

Trypanosoma brucei cells express another protein, TbRbp38 (p38), which shares several major biochemical and functional features with TbUMSBP2 and may also play a role in the crosstalk between the two subcellular genomes. Rbp38 was initially described in *Leishmania tarentolae* and *T. brucei* as an RNA-binding protein that stabilizes RNA in the mitochondria (65). The *Trypanosoma cruzi* homolog (Tc38) was identified as a protein that binds stretches of poly (dT–dG) (66). Remarkably, Liu *et al.* (23) have found that TbRbp38 binds specifically the UMS sequence as well as an oligonucleotide containing a conserved hexamer sequence (the two conserved sequences associated with the replication origins of the kDNA minicircle), similarly to previous reports on the mitochondrial DNA binding targets of UMSBP (30,35). Silencing of *TbRBP38* resulted in the loss of kDNA minicircles and maxicircles, as well as of free minicircle replication intermediates, indicating a role for this protein in kDNA replication (23). Significantly, in addition to their similar roles in mitochondrial DNA replication, both proteins, TbUMSBP2 and Rbp38, also appear to target a similar nuclear sequence. Lira *et al.* (10,21) reported that the *L. amazonensis* Rbp38

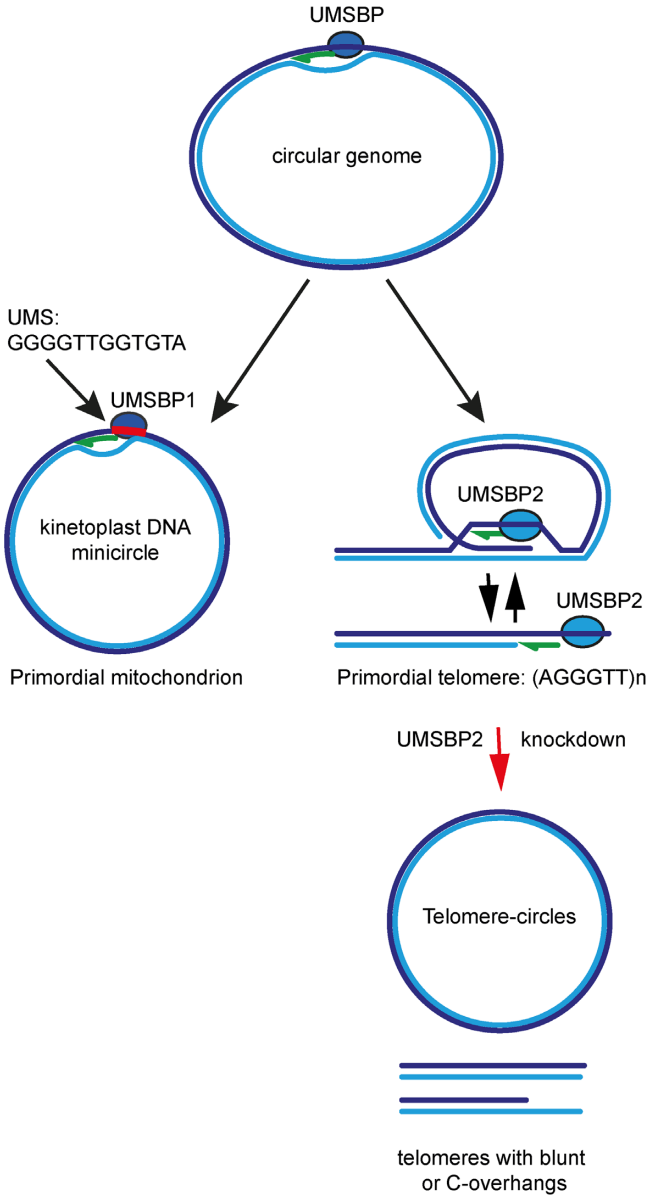

Figure 9. A hypothetical model for the role of UMSBP in the evolution of linear chromosomes with primordial telomeres from a circular genome. An ancestor UMSBP-type protein played a role in the maintenance of an ancestral circular genome. As early eukaryotes evolved, two UMSBP paralogs were adapted to maintain the primordial telomeres in the nucleus and the circular genome of the mitochondria by binding to the G-rich single stranded telomeric DNA or UMS, respectively. UMSBP2 knockdown results in the de-protection of telomeres, as shown by a reduction in the G-overhang and an increase in C-overhang and excised t-circles, a portion of them may be gapped or nicked in the G-strand (C-circles) or the C-strand (G-circles).

homologue (LaRbp38) binds the G-rich single-stranded telomeric DNA *in vitro*, and immunoprecipitates with both the kinetoplast and nuclear DNA in ChIP analysis. How Rbp38, which predominantly localizes to the cell mitochondrion, is also targeted to the nucleus, is still unknown. If TbUMSBP2 functions directly in the mitochondrion, it may represent the reciprocal case to that of Rbp38, where a protein that predominantly localizes to the nucleus and interacts with telomeres, also functions in mitochondrial DNA replication and segregation (40). In addition to the TbUMSBP2 and Rbp38 proteins discussed above, another replication protein, RPA-1 from *L. amazonensis* (LaRPA-1) has been reported to interact with telomeres (67). Recent reports indicated that *T. cruzi* RPA1 (TcRPA-1) binds single stranded DNA *in vitro*, with preference to the telomeric G-rich sequence (68,69). TcRPA-1 colocalizes with telomeres also beyond S/G2 phases, suggesting that it may play other roles in DNA metabolism in addition to its functions in DNA replication (69).

Telomeres are essential nucleoprotein complexes that protect the ends of the linear eukaryotic chromosomes from degradation and distinguish them from double-strand breaks, which normally activate the potent DDR and repair mechanisms (1). The telomere end can serve as a substrate for DNA polymerases (including telomerase), nucleases, helicases, DDR sensors, recombination machinery, NHEJ machinery, etc. Specialized proteins that bind the telomere ends are in a strategic position to coordinate these activities and achieve a delicate balance between telomere elongation and shortening. A number of proteins were found to bind the conserved telomeric 3′ overhang (70), such as POT1 in mammals and *Schizosaccharomyces pombe,* the trimeric CST complex in mammals and budding yeast, and TEBP α and β in ciliates (reviewed in (71)). TEBPα was shown to tether telomeres to a nuclear structure (72). In *C. elegans*, both G-rich 3′ overhangs and C-rich 5′ overhangs were identified, which are bound by CeOB1/POT-2 and CeOB2/POT-1, respectively (64). All known telomeric ssDNA binding proteins have an oligonucleotide/oligosaccharide (OB)-fold that facilitates the specific interaction with the single-stranded telomeric sequence. Here we report that TbUMSBP2 is a telomeric ssDNA binding protein, which is essential for telomere function. Yet, similarly to the recently described TZAP (8), TbUMSBP2 is not an OB-fold but a zinc-finger protein. While TZAP binds double-stranded DNA, TbUMSBP2 binds exclusively to single-stranded (G-rich) telomeric sequence. It contains 7 CCHC-type zinc fingers, which mediate the specific interaction with the telomeric ssDNA. Depletion of TbUMSBP2 affected the telomere arrangement in the nucleus, leading to their clustering in one or more foci (Figure 3). It also caused the activation of DDR in the vicinity of the telomeres, as revealed by H2A phosphorylation and the formation of large γH2A foci colocalizing with the telomeres (Figure 4), consistent with the functions reported for other telomeric overhang binding proteins such as TEBPα (72).

Interestingly, in WT *T. brucei* cells we observed both G-rich and C-rich single-stranded telomeric overhangs (Figures 5–7; Supplementary Figures S3–5), as found in *C. elegans* (64). Remarkably, we also observed a significant amount of linear and circular ECTRs with at least some single-stranded regions (Figure 6). TbUMSBP2 depletion reduced the G-rich overhangs and single-stranded fragments and increased the C-rich overhangs and single stranded fragments (Figures 5 and 7; Supplementary Figures S3 and S4). RNAi knockdown of *TRF* in *T. brucei* resulted in a similar phenotype—an immediate cell cycle arrest, mostly in S phase but also in G2/M, and an immediate

reduction in the telomeric G-overhang signal observed by RAGE followed by in-gel hybridization (18). In mammals, aberrant resolution of the t-loop structure upon telomere deprotection by the expression of a dominant negative mutant of the telomere protein TRF2 has two distinct consequences: release of circular telomeric dsDNA (t-circles) and formation of 5′ C-rich overhangs (62,63). Therefore, we hypothesized that the increased C-overhangs may be associated with the formation of t-circles. We tested the formation of t-circles that are gapped or nicked on one strand (C-circles or G-circles) by 2D gel electrophoresis and native and denatured hybridization (Figures 6 and 7; Supplementary Figure S6), and by ϕ29 DNA polymerase rolling circle amplification assay (Figure 8; Supplementary Figures S7 and 8). Interestingly, both C- and G-circles exist in uninduced procyclic *T. brucei* cells, suggesting that telomeres in these cells do not fully repress t-circle formation, perhaps as a telomere-trimming mechanism that is used to regulate telomere length (63,73,74). Unlike human ALT cells, which predominantly generate C-circles, both C- and G-circles increased significantly upon TbUMSBP2 depletion, suggesting that TbUMSBP2 plays a role in the restriction of t-loop excision. Notably, the background level of t-circles observed in WT trypanosomes may also be consistent with the observations that repetitive DNA sequences, including tandem repeats at telomeres, centromeres and rDNA, can form extrachromosomal circular DNA (eccDNA), which are ubiquitous in all eukaryotic genomes examined (reviewed in (75)).

It was hypothesized that when linear genomes evolved from circular genomes in early eukaryotes, the recombination machinery was recruited to form t-loops and facilitate both telomere capping and length maintenance (76). Later in evolution, this ancestral telomere protection and maintenance mechanism gave way to specialized proteins and t-loop structure that cap the telomere, and to telomerase, which elongates it. In line with this evolutionary scheme, when the linear genomes appeared and a single stranded DNA binding protein was needed to protect the G-rich 3′ overhang or a displaced G-strand within a t-loop, and regulate telomere synthesis, an existing UMSBP paralog was adapted to function in the nucleus (Figure 9). Rapid evolution of telomere binding protein through paralog formation was hypothesized before (77). In line with this hypothesis, no OB-fold single-stranded telomeric binding proteins were found so far in *T. brucei,* while proteins such as TEBPα, Cdc13 and POT1 have evolved later in other organisms. These OB-fold proteins co-evolved with other telomere factors, specialized better in telomere end protection and replaced UMSBP. In early evolving eukaryotes such as trypanosomes, t-loops may have not yet fully stabilized as a capping structure and telomerase may have not yet been strictly regulated to maintain constant telomere length. Thus, in trypanosomes, t-loops resolution and t-circle excision may serve a more dominant role in telomere length regulation, than that found in yeast and mammalian cells (73,74). Further study of the UMSBP proteins and their roles in the replication and maintenance of the mitochondrial and nuclear genomes will enhance the understanding of the evolution of linear genomes with telomeres from the more ancient circular genomes.

SUPPLEMENTARY DATA

Supplementary Data are available at NAR Online.

ACKNOWLEDGEMENTS

We thank Dr George A.M. Cross for the generous gift of plasmid pMOTag2H, and Drs David Horn and Lucy Glover for the generous gift of anti-γH2A antibodies.

FUNDING

United States-Israel Binational Science Foundation [2011156 to J.S., 2013344 to Y.T.]; Israel Science Foundation [1127/10, 1021/14 to J.S., 1729/13 to Y.T.]; Worldwide Cancer Research [15-0338 to Y.T.]. Funding for open access charge: Israel Science Foundation [1021/14 to J.S.]; Worldwide Cancer Research [15-0338 to Y.T.].
Conflict of interest statement. None declared.

REFERENCES

1. Jain,D. and Cooper,J.P. (2010) Telomeric strategies: means to an end. *Annu. Rev. Genet.*, **44**, 243–269.
2. Griffith,J.D., Comeau,L., Rosenfield,S., Stansel,R.M., Bianchi,A., Moss,H. and de Lange,T. (1999) Mammalian telomeres end in a large duplex loop. *Cell*, **97**, 503–514.
3. Ferreira,H.C., Towbin,B.D., Jegou,T. and Gasser,S.M. (2013) The shelterin protein POT-1 anchors Caenorhabditis elegans telomeres through SUN-1 at the nuclear periphery. *J. Cell Biol.*, **203**, 727–735.
4. Giraud-Panis,M.J., Teixeira,M.T., Geli,V. and Gilson,E. (2010) CST meets shelterin to keep telomeres in check. *Mol. Cell*, **39**, 665–676.
5. Hockemeyer,D., Sfeir,A.J., Shay,J.W., Wright,W.E. and de Lange,T. (2005) POT1 protects telomeres from a transient DNA damage response and determines how human chromosomes end. *EMBO J.*, **24**, 2667–2678.
6. Shtessel,L., Lowden,M.R., Cheng,C., Simon,M., Wang,K. and Ahmed,S. (2013) Caenorhabditis elegans POT-1 and POT-2 repress telomere maintenance pathways. *G3*, **3**, 305–313.
7. Croy,J.E. and Wuttke,D.S. (2006) Themes in ssDNA recognition by telomere-end protection proteins. *Trends Biochem. Sci.*, **31**, 516–525.
8. Li,J.S., Miralles Fuste,J., Simavorian,T., Bartocci,C., Tsai,J., Karlseder,J. and Lazzerini Denchi,E. (2017) TZAP: A telomere-associated protein involved in telomere length control. *Science*, **355**, 638–641.
9. Dreesen,O., Li,B. and Cross,G.A. (2007) Telomere structure and function in trypanosomes: a proposal. *Nat. Rev. Microbiol.*, **5**, 70–75.
10. Lira,C.B., Giardini,M.A., Neto,J.L., Conte,F.F. and Cano,M.I. (2007) Telomere biology of trypanosomatids: beginning to answer some questions. *Trends Parasitol.*, **23**, 357–362.
11. Kuprys,P.V., Davis,S.M., Hauer,T.M., Meltser,M., Tzfati,Y. and Kirk,K.E. (2013) Identification of telomerase RNAs from filamentous fungi reveals conservation with vertebrates and yeasts. *PLoS One*, **8**, e58661.
12. Munoz-Jordan,J.L., Cross,G.A., de Lange,T. and Griffith,J.D. (2001) t-loops at trypanosome telomeres. *EMBO J.*, **20**, 579–588.
13. DuBois,K.N., Alsford,S., Holden,J.M., Buisson,J., Swiderski,M., Bart,J.M., Ratushny,A.V., Wan,Y., Bastin,P., Barry,J.D. *et al.* (2012) NUP-1 Is a large coiled-coil nucleoskeletal protein in trypanosomes with lamin-like functions. *PLoS Biol.*, **10**, e1001287.
14. Horn,D. and McCulloch,R. (2010) Molecular mechanisms underlying the control of antigenic variation in African trypanosomes. *Curr. Opin. Microbiol.*, **13**, 700–705.
15. Field,M.C., Horn,D., Alsford,S., Koreny,L. and Rout,M.P. (2012) Telomeres, tethers and trypanosomes. *Nucleus*, **3**, 478–486.
16. Glover,L., Hutchinson,S., Alsford,S., McCulloch,R., Field,M.C. and Horn,D. (2013) Antigenic variation in African trypanosomes: the importance of chromosomal and nuclear context in VSG expression control. *Cell. Microbiol.*, **15**, 1984–1993.
17. Horn,D. (2014) Antigenic variation in African trypanosomes. *Mol. Biochem. Parasitol.*, **195**, 123–129.

18. Li,B. (2015) DNA double-strand breaks and telomeres play important roles in trypanosoma brucei antigenic variation. *Eukaryot. Cell*, **14**, 196–205.
19. Li,B., Espinal,A. and Cross,G.A. (2005) Trypanosome telomeres are protected by a homologue of mammalian TRF2. *Mol. Cell. Biol.*, **25**, 5011–5021.
20. Yang,X., Figueiredo,L.M., Espinal,A., Okubo,E. and Li,B. (2009) RAP1 is essential for silencing telomeric variant surface glycoprotein genes in Trypanosoma brucei. *Cell*, **137**, 99–109.
21. Lira,C.B., Siqueira Neto,J.L., Giardini,M.A., Winck,F.V., Ramos,C.H. and Cano,M.I. (2007) LaRbp38: a Leishmania amazonensis protein that binds nuclear and kinetoplast DNAs. *Biochem. Biophys. Res. Commun.*, **358**, 854–860.
22. Neto,J.L., Lira,C.B., Giardini,M.A., Khater,L., Perez,A.M., Peroni,L.A., dos Reis,J.R., Freitas-Junior,L.H., Ramos,C.H. and Cano,M.I. (2007) Leishmania replication protein A-1 binds in vivo single-stranded telomeric DNA. *Biochem. Biophys. Res. Commun.*, **358**, 417–423.
23. Liu,B., Molina,H., Kalume,D., Pandey,A., Griffith,J.D. and Englund,P.T. (2006) Role of p38 in replication of Trypanosoma brucei kinetoplast DNA. *Mol. Cell. Biol.*, **26**, 5382–5393.
24. Shlomai,J. (2004) The structure and replication of kinetoplast DNA. *Curr. Mol. Med.*, **4**, 623–647.
25. Lukes,J., Hashimi,H. and Zikova,A. (2005) Unexplained complexity of the mitochondrial genome and transcriptome in kinetoplastid flagellates. *Curr. Genet.*, **48**, 277–299.
26. Liu,B., Liu,Y., Motyka,S.A., Agbo,E.E. and Englund,P.T. (2005) Fellowship of the rings: the replication of kinetoplast DNA. *Trends Parasitol.*, **21**, 363–369.
27. Jensen,R.E. and Englund,P.T. (2012) Network news: the replication of kinetoplast DNA. *Annu. Rev. Microbiol.*, **66**, 473–491.
28. Bezalel-Buch,R., Yaffe,N. and Shlomai,J. (2013) Replication machinery of kinetoplast DNA In: Jäger,T, Koch,O and Flohé,L (eds). *Trypanosomatid diseases: molecular routes to drug discovery*. 1st edn. Wiley-VCH Verlag GmbH & Co. KGaA, Weinheim, pp. 243–260.
29. Abu-Elneel,K., Robinson,D.R., Drew,M.E., Englund,P.T. and Shlomai,J. (2001) Intramitochondrial localization of universal minicircle sequence-binding protein, a trypanosomatid protein that binds kinetoplast minicircle replication origins. *J. Cell Biol.*, **153**, 725–734.
30. Abu-Elneel,K., Kapeller,I. and Shlomai,J. (1999) Universal minicircle sequence-binding protein, a sequence-specific DNA-binding protein that recognizes the two replication origins of the kinetoplast DNA minicircle. *J. Biol. Chem.*, **274**, 13419–13426.
31. Tzfati,Y. and Shlomai,J. (1998) Genomic organization and expression of the gene encoding the universal minicircle sequence binding protein. *Mol. Biochem. Parasitol.*, **94**, 137–141.
32. Tzfati,Y., Abeliovich,H., Avrahami,D. and Shlomai,J. (1995) Universal minicircle sequence binding protein, a CCHC-type zinc finger protein that binds the universal minicircle sequence of trypanosomatids. Purification and characterization. *J. Biol. Chem.*, **270**, 21339–21345.
33. Avrahami,D., Tzfati,Y. and Shlomai,J. (1995) A single-stranded DNA binding protein binds the origin of replication of the duplex kinetoplast DNA. *Proc. Natl. Acad. Sci. U.S.A.*, **92**, 10511–10515.
34. Abeliovich,H., Tzfati,Y. and Shlomai,J. (1993) A trypanosomal CCHC-type zinc finger protein which binds the conserved universal sequence of kinetoplast DNA minicircles: isolation and analysis of the complete cDNA from Crithidia fasciculata. *Mol. Cell. Biol.*, **13**, 7766–7773.
35. Tzfati,Y., Abeliovich,H., Kapeller,I. and Shlomai,J. (1992) A single-stranded DNA-binding protein from Crithidia fasciculata recognizes the nucleotide sequence at the origin of replication of kinetoplast DNA minicircles. *Proc. Natl. Acad. Sci. U.S.A.*, **89**, 6891–6895.
36. Onn,I., Kapeller,I., Abu-Elneel,K. and Shlomai,J. (2006) Binding of the universal minicircle sequence binding protein at the kinetoplast DNA replication origin. *J. Biol. Chem.*, **281**, 37468–37476.
37. Sela,D. and Shlomai,J. (2009) Regulation of UMSBP activities through redox-sensitive protein domains. *Nucleic Acids Res.*, **37**, 279–288.
38. Sela,D., Yaffe,N. and Shlomai,J. (2008) Enzymatic mechanism controls redox-mediated protein-DNA interactions at the replication origin of kinetoplast DNA minicircles. *J. Biol. Chem.*, **283**, 32034–32044.
39. Onn,I., Milman-Shtepel,N. and Shlomai,J. (2004) Redox potential regulates binding of universal minicircle sequence binding protein at the kinetoplast DNA replication origin. *Eukaryot. Cell*, **3**, 277–287.
40. Milman,N., Motyka,S.A., Englund,P.T., Robinson,D. and Shlomai,J. (2007) Mitochondrial origin-binding protein UMSBP mediates DNA replication and segregation in trypanosomes. *Proc. Natl. Acad. Sci. U.S.A.*, **104**, 19250–19255.
41. Singh,R., Purkait,B., Abhishek,K., Saini,S., Das,S., Verma,S., Mandal,A., Ghosh,A.K., Ansari,Y., Kumar,A. *et al.* (2016) Universal minicircle sequence binding protein of Leishmania donovani regulates pathogenicity by controlling expression of cytochrome-b. *Cell Biosci.*, **6**, 13.
42. Drew,M.E. and Englund,P.T. (2001) Intramitochondrial location and dynamics of Crithidia fasciculata kinetoplast minicircle replication intermediates. *J. Cell Biol.*, **153**, 735–744.
43. Ploubidou,A., Robinson,D.R., Docherty,R.C., Ogbadoyi,E.O. and Gull,K. (1999) Evidence for novel cell cycle checkpoints in trypanosomes: kinetoplast segregation and cytokinesis in the absence of mitosis. *J. Cell Sci.*, **112**, 4641–4650.
44. Liu,B., Wang,J., Yaffe,N., Lindsay,M.E., Zhao,Z., Zick,A., Shlomai,J. and Englund,P.T. (2009) Trypanosomes have six mitochondrial DNA helicases with one controlling kinetoplast maxicircle replication. *Mol. Cell*, **35**, 490–501.
45. Wang,Z., Morris,J.C., Drew,M.E. and Englund,P.T. (2000) Inhibition of Trypanosoma brucei gene expression by RNA interference using an integratable vector with opposing T7 promoters. *J. Biol. Chem.*, **275**, 40174–40179.
46. Oberholzer,M., Morand,S., Kunz,S. and Seebeck,T. (2006) A vector series for rapid PCR-mediated C-terminal in situ tagging of Trypanosoma brucei genes. *Mol Biochem Parasitol*, **145**, 117–120.
47. DeGrasse,J.A., Chait,B.T., Field,M.C. and Rout,M.P. (2008) High-yield isolation and subcellular proteomic characterization of nuclear and subnuclear structures from trypanosomes. *Methods Mol. Biol.*, **463**, 77–92.
48. Lamm,N., Ordan,E., Shponkin,R., Richler,C., Aker,M. and Tzfati,Y. (2009) Diminished telomeric 3′ overhangs are associated with telomere dysfunction in Hoyeraal-Hreidarsson syndrome. *PLoS One*, **4**, e5666.
49. Wang,R.C., Smogorzewska,A. and de Lange,T. (2004) Homologous recombination generates T-loop-sized deletions at human telomeres. *Cell*, **119**, 355–368.
50. Henson,J.D., Cao,Y., Huschtscha,L.I., Chang,A.C., Au,A.Y., Pickett,H.A. and Reddel,R.R. (2009) DNA C-circles are specific and quantifiable markers of alternative-lengthening-of-telomeres activity. *Nat. Biotechnol.*, **27**, 1181–1185.
51. Perez-Morga,D., Amiguet-Vercher,A., Vermijlen,D. and Pays,E. (2001) Organization of telomeres during the cell and life cycles of Trypanosoma brucei. *J. Eukaryot. Microbiol.*, **48**, 221–226.
52. Glover,L. and Horn,D. (2012) Trypanosomal histone gammaH2A and the DNA damage response. *Mol. Biochem. Parasitol.*, **183**, 78–83.
53. Glover,L., Alsford,S. and Horn,D. (2013) DNA break site at fragile subtelomeres determines probability and mechanism of antigenic variation in African trypanosomes. *PLoS Pathog.*, **9**, e1003260.
54. Elderkin,S., Maertens,G.N., Endoh,M., Mallery,D.L., Morrice,N., Koseki,H., Peters,G., Brockdorff,N. and Hiom,K. (2007) A phosphorylated form of Mel-18 targets the Ring1B histone H2A ubiquitin ligase to chromatin. *Mol. Cell*, **28**, 107–120.
55. Ikura,T., Tashiro,S., Kakino,A., Shima,H., Jacob,N., Amunugama,R., Yoder,K., Izumi,S., Kuraoka,I., Tanaka,K. *et al.* (2007) DNA damage-dependent acetylation and ubiquitination of H2AX enhances chromatin dynamics. *Mol. Cell Biol.*, **27**, 7028–7040.
56. van Attikum,H. and Gasser,S.M. (2009) Crosstalk between histone modifications during the DNA damage response. *Trends Cell Biol.*, **19**, 207–217.
57. Pan,M.R., Peng,G., Hung,W.C. and Lin,S.Y. (2011) Monoubiquitination of H2AX protein regulates DNA damage response signaling. *J. Biol. Chem.*, **286**, 28599–28607.
58. Chen,L.Y. and Lingner,J. (2013) CST for the grand finale of telomere replication. *Nucleus*, **4**, 277–282.
59. Chen,L.Y., Majerska,J. and Lingner,J. (2013) Molecular basis of telomere syndrome caused by CTC1 mutations. *Genes Dev.*, **27**, 2099–2108.

60. Simon,A.J., Lev,A., Zhang,Y., Weiss,B., Rylova,A., Eyal,E., Kol,N., Barel,O., Cesarkas,K., Soudack,M. *et al.* (2016) Mutations in STN1 cause Coats plus syndrome and are associated with genomic and telomere defects. *J. Exp. Med.*, **213**, 1429–1440.
61. Janzen,C.J., Lander,F., Dreesen,O. and Cross,G.A. (2004) Telomere length regulation and transcriptional silencing in KU80-deficient Trypanosoma brucei. *Nucleic Acids Res.*, **32**, 6575–6584.
62. Oganesian,L. and Karlseder,J. (2011) Mammalian 5′ C-rich telomeric overhangs are a mark of recombination-dependent telomere maintenance. *Mol. Cell*, **42**, 224–236.
63. Oganesian,L. and Karlseder,J. (2013) 5′ C-rich telomeric overhangs are an outcome of rapid telomere truncation events. *DNA Repair (Amst)*, **12**, 238–245.
64. Raices,M., Verdun,R.E., Compton,S.A., Haggblom,C.I., Griffith,J.D., Dillin,A. and Karlseder,J. (2008) C. elegans telomeres contain G-strand and C-strand overhangs that are bound by distinct proteins. *Cell*, **132**, 745–757.
65. Sbicego,S., Alfonzo,J.D., Estevez,A.M., Rubio,M.A., Kang,X., Turck,C.W., Peris,M. and Simpson,L. (2003) RBP38, a novel RNA-binding protein from trypanosomatid mitochondria, modulates RNA stability. *Eukaryot. Cell*, **2**, 560–568.
66. Duhagon,M.A., Dallagiovanna,B., Ciganda,M., Ruyechan,W., Williams,N. and Garat,B. (2003) A novel type of single-stranded nucleic acid binding protein recognizing a highly frequent motif in the intergenic regions of Trypanosoma cruzi. *Biochem. Biophys. Res. Commun.*, **309**, 183–188.
67. Fernandez,M.F., Castellari,R.R., Conte,F.F., Gozzo,F.C., Sabino,A.A., Pinheiro,H., Novello,J.C., Eberlin,M.N. and Cano,M.I. (2004) Identification of three proteins that associate in vitro with the Leishmania (Leishmania) amazonensis G-rich telomeric strand. *Eur. J. Biochem.*, **271**, 3050–3063.
68. Pavani,R.S., da Silva,M.S., Fernandes,C.A., Morini,F.S., Araujo,C.B., Fontes,M.R., Sant'Anna,O.A., Machado,C.R., Cano,M.I., Fragoso,S.P. *et al.* (2016) Replication protein A presents canonical functions and is also involved in the differentiation capacity of trypanosoma cruzi. *PLoS Negl. Trop. Dis.*, **10**, e0005181.
69. Pavani,R.S., Vitarelli,M.O., Fernandes,C.A.H., Mattioli,F.F., Morone,M., Menezes,M.C., Fontes,M.R.M., Cano,M.I.N. and Elias,M.C. (2017) Replication protein A-1 has a preference for the telomeric G-rich sequence in trypanosoma cruzi. *J. Eukaryot. Microbiol.*, **65**, 345–356.
70. Henderson,E.R. and Blackburn,E.H. (1989) An overhanging 3′ terminus is a conserved feature of telomeres. *Mol. Cell. Biol.*, **9**, 345–348.
71. Dickey,T.H., Altschuler,S.E. and Wuttke,D.S. (2013) Single-stranded DNA-binding proteins: multiple domains for multiple functions. *Structure*, **21**, 1074–1084.
72. Paeschke,K., Juranek,S., Rhodes,D. and Lipps,H.J. (2008) Cell cycle-dependent regulation of telomere tethering in the nucleus. *Chromosome Res.*, **16**, 721–728.
73. Li,B. and Lustig,A.J. (1996) A novel mechanism for telomere size control in Saccharomyces cerevisiae. *Genes Dev.*, **10**, 1310–1326.
74. Pickett,H.A., Henson,J.D., Au,A.Y.M., Neumann,A.A. and Reddel,R.R. (2011) Normal mammalian cells negatively regulate telomere length by telomere trimming. *Hum. Mol. Genet.*, **20**, 4684–4692.
75. Cohen,S. and Segal,D. (2009) Extrachromosomal circular DNA in eukaryotes: possible involvement in the plasticity of tandem repeats. *Cytogenet. Genome Res.*, **124**, 327–338.
76. de Lange,T. (2004) T-loops and the origin of telomeres. *Nat. Rev. Mol. Cell Biol.*, **5**, 323–329.
77. Lustig,A.J. (2016) Hypothesis: Paralog formation from progenitor proteins and paralog mutagenesis spur the rapid evolution of telomere binding proteins. *Front. Genet.*, **7**, 10.